Thermomechanical model for evaluation of the superelastic response of NiTi shape memory alloys under dynamic conditions

2013 Smart Mater. Struct. 22 035017

(http://iopscience.iop.org/0964-1726/22/3/035017)

IOP Publishing Smart Materials and Structures
Smart Mater. Struct. **22** (2013) 035017 (13pp) doi:10.1088/0964-1726/22/3/035017

Thermomechanical model for evaluation of the superelastic response of NiTi shape memory alloys under dynamic conditions

H Soul[1] **and A Yawny**[1,2]

[1] CONICET, División Metales, Centro Atómico Bariloche (CNEA), Instituto Balseiro (UNCuyo), Avenida Bustillo 9500, (8400) San Carlos de Bariloche, Argentina
[2] CNEA, División Metales, Centro Atómico Bariloche (CNEA), Instituto Balseiro (UNCuyo), Avenida Bustillo 9500, (8400) San Carlos de Bariloche, Argentina

E-mail: soulh@ib.cnea.gov.ar

Received 14 August 2012, in final form 27 December 2012
Published 14 February 2013
Online at stacks.iop.org/SMS/22/035017

Abstract
The development of a 1D thermomechanical model for simulating the response of uniaxial superelastic NiTi elements is described. The formulation of the model includes consideration of the dependence of the critical stresses for forward and reverse transformation on the temperature, the occurrence of strain rate effects due to self-heating/cooling associated with the latent heat of the stress induced martensitic transformation, the localized character of the stress induced transformation in superelastic NiTi wires and ribbons, the possibility of nucleation events during both the forward and reverse transformations and the occurrence of non-recoverable residual strains. Numerical simulations allowed rationalization of different features commonly observed in experiments and their dependence on strain rate and environment conditions. Comparisons of numerical results with experimental cycles obtained in the present work and also with data published in the literature indicate the potentiality of the developed model as a design tool for simulating the response of superelastic materials subjected to realistic service conditions.

(Some figures may appear in colour only in the online journal)

1. Introduction

Superelasticity is one of the distinguishing effects exhibited by shape memory alloys (SMAs) [1]. It is the capacity exhibited by these materials to deform under the application of a mechanical load to approximately 10% strain in a nearly reversible manner. Responsible for this peculiar behavior is the existence in these materials of a stress induced martensitic phase transformation from an austenitic phase (A) to a martensite phase (M). In the case of single crystalline or polycrystalline (quasi-) unidimensional specimens, i.e. wires, strips, and bars, transformation takes place once a critical transformation stress $\sigma_{A–M}$ is reached. Upon unloading, the transformation reverts, and this occurs at a stress $\sigma_{M–A}$ lower than $\sigma_{A–M}$. The original specimen dimensions are recovered in this way [2]. The stress hysteresis defined as $\Delta\sigma = \sigma_{A–M} - \sigma_{M–A}$ gives rise to energy dissipation, which, in the case of a complete cycle, can be assessed by the area enclosed by the σ–ε trajectory. It is precisely due to this energy dissipation capability that SMAs have been considered potential candidates as damping elements in a variety of structures subjected to dynamical loadings [3–6].

Among the broad range of shape memory alloys, Cu based and NiTi alloys comprise the widely studied groups [7, 8]. Near-equiatomic NiTi alloys have reached higher technological relevance due to the excellent combination of properties such as high transformation stress, high level of strain recovery, adequate fatigue life, and excellent wear and corrosion resistance, including biocompatibility [9]. Nowadays these qualities can be found in commercially available NiTi materials shaped as wires or ribbons and obtained via appropriate thermomechanical procedures.

Studies of the superelastic behavior of NiTi specimens can be roughly classified into those focused on the understanding of the mechanisms behind the effect and those devoted to the characterization of the relevant aspects associated with specific applications. Among the former is the phenomenon of the localization of the transformation. The forward transformation (A → M) proceeds by the advance of distinct interfaces; i.e., once a martensite domain has nucleated, further straining of the specimen results in A/M interfaces propagating along the specimen. The phenomenon resembles Lüders band propagation observed during plastic deformation of low carbon steels [10, 11]. The reverse transformation (M → A) exhibits the same character, with interfaces reverting upon unloading. Although there is no complete consensus about the causes of such a behavior [12, 13], the dimensional mismatch at the interface between austenite and martensite phases could play a significant role. In effect, in order to maintain displacement field continuity, a triaxial stress state is generated at this interface. This will in turn result in an increased local effective stress, which will concentrate the transformation activity in this region. In this way, the local development of both the forward and reverse transformations [14, 15] is enhanced. In low strain rate (quasi-static) experiments, only one or two interfaces moving along the specimen are usually observed. Under such conditions, the interface movement can be easily tracked [16] and an analysis of the microstructural evolution and major fatigue damage must be limited to those sections of the specimen that have been swept by the interface movement. As strain rate is increased, the experimental evidence indicates that the number of transformation domains multiplies. For example, Zhang *et al* [17] have found a one-half power exponent dependence of the number of fronts on the strain rate in experiments performed in NiTi strips.

Another important aspect from the point of view of any application involving SMA superelasticity is the temperature dependence of the critical stresses $\sigma_{A–M}$ and $\sigma_{M–A}$. A thermodynamic analysis applied to martensitic phase transformation in stressed solids indicates that this relationship can be expressed as a Clausius–Clapeyron type of relation which gives the slope $d\sigma/dT = \beta$ in terms of the entropy change and the strain change associated with the transformation [2]. The temperature dependence of the critical stresses can be determined experimentally with typical values of β ranging from 6 to 7 MPa K^{-1} for NiTi SMAs [18]. This coupling between temperature and critical transformation stress results in a dependence of the mechanical response on the strain rate, the ambient temperature and the heat transfer characteristics between specimen and surroundings. This, in turn, is reflected in the mechanical σ–ε behavior, which departs from that observed under isothermal conditions (quasi-static straining). Therefore, a proper assessment of the material response under dynamic conditions, such as those associated with damping applications, must necessarily include the coupling between the mentioned effects. Results such as those in [19–22] reporting a non-monotonic dependence of the dissipated energy on the strain rate (or cycling frequency) and the existence of a strain rate for which the energy dissipation is maximized can only be rationalized in terms of the thermomechanical coupling described before. The development of a model able to describe the behavior of SMA elements during dynamic conditions is thus highly desirable. Independently of the pursued aims, the models proposed to date range from simple mechanical behavior laws derived from fitted experimental curves to complex constitutive models with which it is possible to address triaxial stress states. Modeling of the superelastic behavior has been exploited as a complementary tool, whether for prediction of the mechanical response of devices aided with superelastic members [23–25], or for studying, analytically or numerically, specific aspects of the associated phenomenology [26, 27]. However, in spite of the thermal effects and the localization phenomena being important aspects to consider in an appropriate description of the mechanical behavior of superelastic NiTi alloys, they are often not adequately considered in model formulations. For example, Heller *et al* [20] and He *et al* [28] studied the self-induced thermal effects with simple models but assuming a homogeneous transformation pattern. In this way the authors attempted to explain the non-monotonic dependence of the hysteresis energy on the strain rate. Maletta *et al* [29] incorporated the temperature dependence of the transformation stresses and developed a zero dimensional thermomechanical model. Morin *et al* [30] proceeded in the same manner based on a 3D model. In both cases, localization was not taken into account or captured by the results, this being a source of error as pointed out in [30]. The importance of considering the localized character of the transformation was assessed by Messner *et al* [31], who studied analytically the temperature profile of a unidimensional NiTi specimen being traversed by a heat releasing interface. From this work, conditions for the isothermal and adiabatic regime as a function of the interface velocity can be estimated. Besides these useful results, analytical expressions are only applicable to forward transformation for the specific boundary conditions, and the conclusions are strictly valid for a fixed number of active interfaces. A more complete approach was achieved by Iadicola *et al* [32], who developed a 3D model. In this case, superelasticity was emulated by a plasticity constitutive relationship, which included a slight softening in the transforming branch followed by a hardening region representing the elastic deformation of the fully martensitic material. The propagation of an interface is obtained as a result of the triaxial stress state arising around it, and the nucleation of new transformation fronts results from the excessive heating. Despite the very good agreement between the simulated and the experimental mechanical responses, the adopted plasticity law is not able to reproduce the reverse transformation path and therefore the cases that can be analyzed are limited to a single forward transformation.

In the present work, the steps involved in the development of a 1D model for the superelastic behavior for NiTi uniaxial specimens are described. Firstly, a simplified model for the mechanical behavior is proposed. It includes the temperature dependence of the transformation stresses via the Clausius–Clapeyron relationship. Secondly, the pure

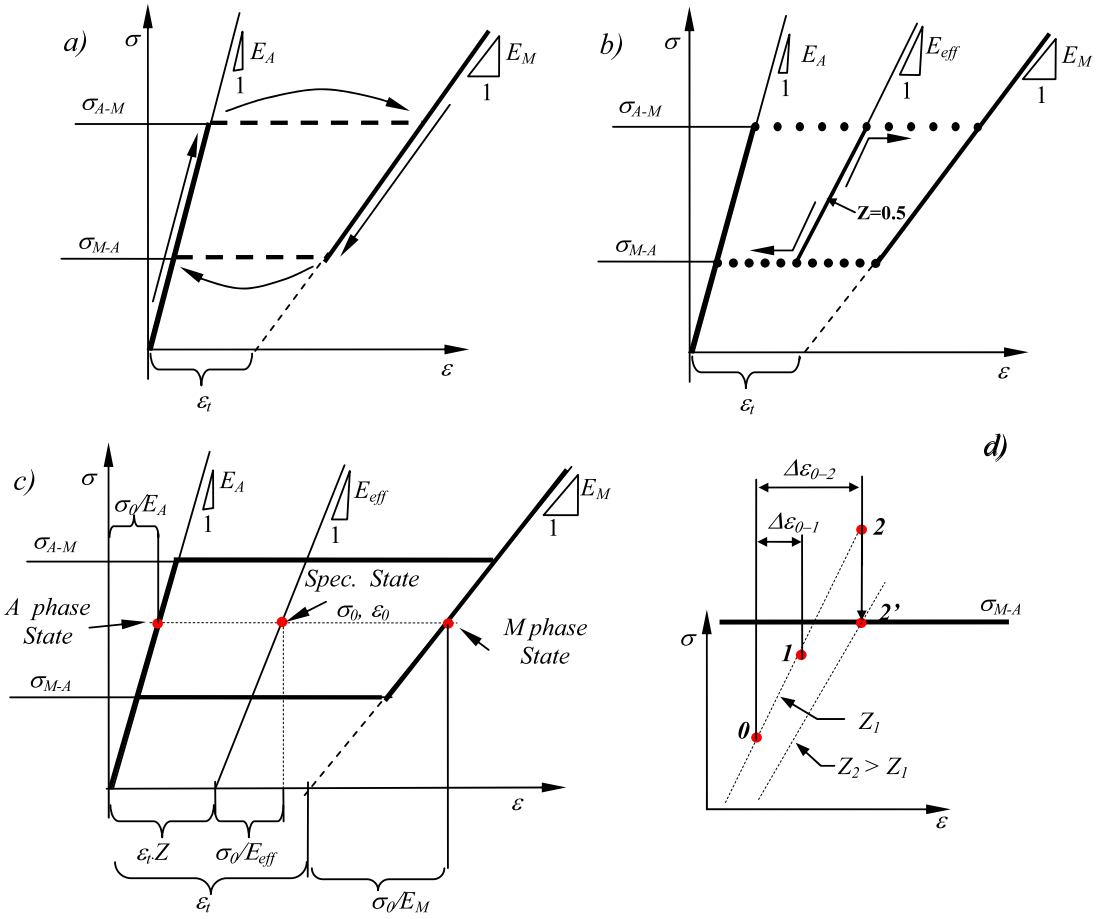

Figure 1. Mechanical model adopted for a uniaxial specimen. (a) States of an elemental volume can be on either the austenitic or martensitic elastic slopes. Jumps from A to M occur at a transformation stress $\sigma_{\mathrm{A–M}}$ and the reverse occurs at the retransformation stress $\sigma_{\mathrm{M–A}}$. (b) σ–ε diagram resulting from an aggregate of $N = 10$ elemental volumes. The martensite phase fraction Z takes discrete values (multiples of $1/N$), as does correspondingly the effective elastic modulus E_{eff}. Transition between Z constant slopes occurs at stress $\sigma_{\mathrm{A–M}}$ ($\sigma_{\mathrm{M–A}}$) upon loading (unloading). (c) σ–ε diagram for a uniaxial superelastic specimen, when N tends to infinity and Z can be assumed to be a continuous variable. (d) Schematic representation of the elastic predictor-transformation corrector rule adopted to evaluate a new state under an applied strain increment.

thermal problem (uncoupled from the mechanical response) associated with the propagation of the transformation interface is addressed. Then, the influence of thermal effects in the superelastic hysteresis is evaluated as a function of the strain rates and environment conditions. Next, the necessity of considering the nucleation of new transforming domains according to the cycling conditions is discussed and a criterion for the nucleation of new transformation domains is proposed. In the next step, the original mechanical model is modified in order to include the localized character of the transformation, the thermomechanical coupling, the possibility of nucleation of new transforming domains and the occurrence of residual strains. The model was then implemented numerically as a first step in the direction of developing a design tool capable of simulation of the complex behavior of superelastic wire materials subjected to realistic service conditions. Finally, the developed model was applied to the study of different benchmark cases in which the strong coupling between the thermal effects, the number of transformation domains and the mechanical response can be appreciated.

2. Basic mechanical uniaxial model

The mechanical model for uniaxial superelastic specimens is derived on the assumption that the material consists of an aggregate of N elemental volumes connected in series. The elements can be either in austenite (A) or martensite (M) phase. Figure 1(a) schematizes the mechanical behavior of such an elemental volume. Under an applied stress σ, the strain ε associated with the elemental volume can be expressed as

$$\varepsilon = \frac{\sigma}{E_{\mathrm{A}}} \tag{1}$$

or

$$\varepsilon = \varepsilon_{\mathrm{t}} + \frac{\sigma}{E_{\mathrm{M}}} \tag{2}$$

depending on whether the element is austenitic, equation (1), or martensitic, equation (2). E_{A} and E_{M} are the austenitic and martensitic elastic moduli, respectively. The term ε_{t} in equation (2) represents the strain associated with the stress induced martensitic phase transformation of the element. The

jump from phase A to phase M occurs at a transformation stress $\sigma_{A\text{–}M}$ upon loading and at a retransformation stress $\sigma_{M\text{–}A}$ upon unloading. Assuming an aggregate of N serial connected elemental volumes, the total uniaxial strain of the specimen can be computed as the mean value of the individual strains as

$$\varepsilon = \frac{\sum_{i=1}^{N} \varepsilon_i}{N} = \frac{N_A}{N}\frac{\sigma}{E_A} + \frac{N_M}{N}\left(\varepsilon_t + \frac{\sigma}{E_M}\right) \tag{3}$$

with N_A and N_M the numbers of austenitic and martensitic elemental volumes, respectively. By defining $Z = N_M/N$, the total martensitic fraction (equivalent to the fraction of elemental volumes in the martensitic state), equation (3) can be rewritten as

$$\begin{aligned}\varepsilon &= (1-Z)\frac{\sigma}{E_A} + Z\left(\varepsilon_t + \frac{\sigma}{E_M}\right)\\ &= \left(\frac{(1-Z)E_M + ZE_A}{E_A E_M}\right)\sigma + Z\varepsilon_t.\end{aligned} \tag{4}$$

The coefficient of the σ-containing term on the right-hand side of (4) can be identified as the inverse of an effective elastic modulus of the specimen E_{eff} defined in terms of the actual Z value:

$$E_{eff}(Z) = \left.\frac{\partial\sigma}{\partial\varepsilon}\right|_Z = \frac{E_A E_M}{E_A Z + E_M(1-Z)}. \tag{5}$$

The behavior of an aggregate of $N = 10$ elemental volumes is represented in figure 1(b). The fact that Z can take only multiples of $1/N$ implies that the transition from A to M and vice versa occurs through discrete states. The jumps of the individual elements from A to M or vice versa are accomplished at stresses $\sigma_{A\text{–}M}$ and $\sigma_{M\text{–}A}$ upon loading or unloading, respectively. If N is high enough, Z can be assumed to be a continuous variable. Now, the pairs $(\sigma;\varepsilon)$ representing all possible states of the specimen are those included and enclosed by the area defined by the two horizontal lines $\sigma_{A\text{–}M}$ and $\sigma_{M\text{–}A}$ and the two inclined lines indicated with slopes E_A and E_M. From (4), an expression for the total martensite fraction Z (now a continuous variable) as a function of σ and ε can be expressed as

$$Z(\sigma,\varepsilon) = \frac{\varepsilon - (\sigma/E_A)}{(\sigma/E_M) - (\sigma/E_A) + \varepsilon_t}. \tag{6}$$

The model can be interpreted graphically with the σ–ε diagram represented in figure 1(c). Here a state $(\sigma_0;\varepsilon_0)$ of the specimen is considered. The constant Z line passing through this point is included in the graph. Its slope corresponds to E_{eff} calculated with (5). The local $(\sigma;\varepsilon)$ states representing fully austenitic condition ($Z = 0$) and fully martensitic condition ($Z = 1$) lie on the lines with slope $E_{eff} = E_A$ and $E_{eff} = E_M$, respectively. Equation (6) therefore works as the level rule used to determine phase fraction from binary phase diagrams. Under externally imposed changes in σ or ε, the specimen behaves elastically unless the evaluated state falls outside the allowed zone given by the lines corresponding to $Z = 0$ and $Z = 1$. The computation of a new state is schematized in figure 1(d). The increment $\Delta\varepsilon_{0-1}$ can be elastically accommodated with an increment $\Delta Z = 0$. If instead the transformation stress is exceeded, as is the case with the increment $\Delta\varepsilon_{0-2}$, the resultant state must be corrected from 2 to 2′ by an increase in the transformed fraction $Z(\Delta Z > 0)$. This rule can be summarized in the following way:

$$\sigma + E_{eff}\Delta\varepsilon > \sigma_{A\text{–}M}, \qquad \Delta Z > 0, \quad \sigma = \sigma_{A\text{–}M} \tag{7}$$

$$\sigma + E_{eff}\Delta\varepsilon < \sigma_{M-A}, \qquad \Delta Z < 0, \quad \sigma = \sigma_{M-A}. \tag{8}$$

Thus, the uniaxial response can be described with the zero-dimensional set of relationships given by equations (4)–(8), without the necessity of considering how the martensite fraction is distributed along the specimen. This simple mechanical model can be improved by considering the temperature dependence of the critical stresses $\sigma_{A\text{–}M}$ and $\sigma_{M\text{–}A}$. Thus, if critical stresses $\sigma_{A\text{–}Mref}$ and $\sigma_{M\text{–}Aref}$ at a reference temperature T_{ref} are known, the critical stresses must be updated to the actual temperature T before computing the next mechanical step according to

$$\sigma_{A\text{–}M} = \sigma_{A\text{–}Mref} + \beta\,(T - T_{ref}) \tag{9}$$

$$\sigma_{M\text{–}A} = \sigma_{M\text{–}Aref} + \beta\,(T - T_{ref})\,. \tag{10}$$

Now, it is necessary to define the temperature T in equations (9) and (10). In quasi-static experiments, it can be assumed that the specimen temperature T is homogeneous along the length of the specimen and equal to the environment temperature T_{amb}. If the process is not quasi-static, temperature changes will be induced due to the effects of the latent heat of transformation. In addition, the temperature will no longer be homogeneous along the length of the specimen, i.e., a temperature profile $T(x)$ will develop. The evaluation of this profile requires consideration of the kinetics of the transformation, which is known to exhibit a localized character in the case of superelastic NiTi. In order to better understand the influence of thermal effects on the superelastic response, in section 3 and before introducing this feature in the model, the temperature changes associated with an interface propagating at different velocities along a NiTi wire specimen are addressed numerically using an uncoupled analysis.

3. Self-induced thermal effects

Thermal effects arising during superelastic cycling have their origin in the latent heat exchange associated with a first order martensitic phase transformation (A → M exothermic; M → A endothermic). Quasi-one-dimensional specimens (wires and ribbons) under typical heat transfer conditions with the surroundings present small Biot numbers relative to the characteristic transversal dimension (diameter) [33]. Therefore, temperature gradients along transverse sections can be neglected. Heat flow is considered to consist of conduction along the longitudinal direction and convection to the ambient media through lateral surface. The balance between the rates of heat generation, accumulation and flow in a differential volume can be represented with the following

1D differential equation:

$$k\frac{\partial^2 T(x,t)}{\partial x^2} + h\frac{P}{A_t}\left(T_{amb} - T(x,t)\right) + L_{at}\dot{Z}(x,t) = \rho C\frac{\partial T(x,t)}{\partial t}. \quad (11)$$

The first term is related to heat conduction along the wire length, k being the thermal conductivity of the material. The second term accounts for heat transferred by convection with the surroundings, which depends on the film coefficient h and the relationship between perimeter P and transverse area A_t. For cylindrical geometries this factor is four times the inverse of the diameter. T_{amb} is the ambient temperature, assumed to be uniform and constant. The third term corresponds to the heat generation rate, which depends on the latent heat of transformation L_{at} and the local rate of phase change $\dot{Z}$. Here, the total latent heat L_{at} is composed by the chemical latent heat (stress free) L_{ch} plus the inelastic work per unit of volume $\sigma\varepsilon_{trans}$, with ε_{trans} being the transformation plateau length [2]. The term on the right represents the sensible heat rate, which depends on the specific heat capacity C and the density of the material ρ. As mentioned before, in NiTi wires and ribbons, a stress induced transformation advances by the propagation of localized interfaces or fronts. For a single interface propagating with a velocity v, the expression describing the magnitude of the local phase change rate can be represented by

$$|\dot{Z}(x,t)| = |v|\delta(x - x_{int}) \quad (12)$$

where δ is the delta Dirac function, indicating that the transformation activity is concentrated at the position of the interface x_{int}. If a number n of interfaces are distributed along the specimen and they move simultaneously, their individual mean velocity can be related to an externally imposed extension velocity V_{ext} through the following expression [10]:

$$\bar{v} \approx \frac{V_{ext}}{n\varepsilon_{trans}}. \quad (13)$$

Equation (13) indicates that the individual front velocity decreases as the number of fronts increases. The problem can be approached analytically, assuming specific cycling conditions and constant number of interfaces (see [31, 32]). In this work, a finite difference scheme was adopted instead, with the aim of extending the analysis to more general situations where the integration of the analytical expressions would be difficult if not impossible to obtain. Therefore, the specimen length and the time are discretized with increments Δx and Δt, respectively. After minor algebraic manipulations, equation (11) is reformulated into the following explicit equation in differences:

$$\Delta T_i^{m+1} = \frac{k}{\rho C}\frac{\Delta t}{\Delta^2 x}\left(T_{i+1}^m - 2T_i^m + T_{i-1}^m\right) + \frac{h}{\rho C}\frac{P}{A_t}\Delta t\left(T_{amb} - T_i^m\right) + \frac{L_{at}}{\rho C}\left(Z_i^{m+1} - Z_i^m\right). \quad (14)$$

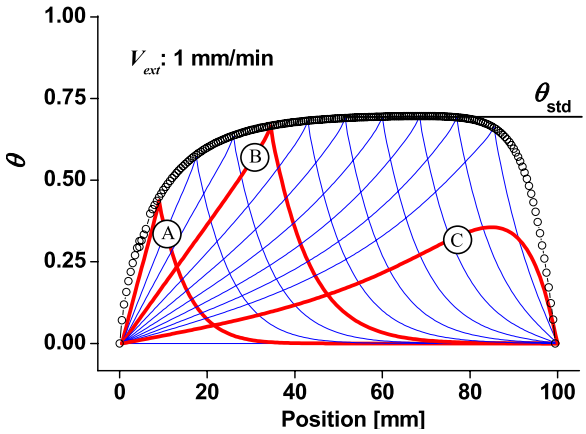

Figure 2. Temperature profiles $\theta(x)$ and trend of θ_{int} obtained for $V_{ext} = 1$ mm min^{-1}.

In this way, the temperature of a node i at instant m is obtained as a function of phase portion change and the temperature in the same and the adjacent volumes corresponding to the previous instant $m - 1$. For this analysis, it is assumed that only one interface can pass through a domain each time the material is transforming. The interface position is evaluated at each instant of time using equation (13). In order to avoid numerical oscillations, Δt must be tuned such that the interface advance in each step is Δx. Another condition that has to be fulfilled by the increments Δt and Δx in order to assure general numerical stability of the explicit method is the following [34]:

$$\frac{k}{\rho C}\frac{\Delta t}{\Delta^2 x} < 0.5. \quad (15)$$

With these thermal considerations in mind, the effects arising during stress induced transformations in superelastic NiTi wires under non-isothermal conditions were studied. Specimens considered have a diameter of 2.5 mm and a length of 100 mm. The following values were adopted for the NiTi properties: $k = 18$ W mK^{-1} (austenite) and 8 W m^{-1} K^{-1} (martensite), $C = 871$ J kg^{-1} K^{-1}, $\rho = 6500$ kg m^{-3} and $L_{at} = 100$ MJ m^{-3} (assumed constant) [32]. The complete plateau strain for the calculus of v was set at 0.06. Temperature changes were normalized by the temperature change associated with the adiabatic condition, i.e., for the situation where the heat of transformation is completely converted into sensible heat:

$$\theta = \frac{T - T_{amb}}{L_{at}/\rho C}. \quad (16)$$

A value $\theta = 1$ thus represents the adiabatic condition which corresponds to a maximum deviation from T_{amb} of 18 K, considering the thermo-physical properties given above.

For the numerical treatment the specimen was represented by a mesh with 200 nodes. The boundary temperatures at the two longitudinal extremes of the wire were fixed at T_{amb} (Dirichlet boundary conditions). Figure 2 shows results obtained for a $V_{ext} = 1$ mm min^{-1} ($v = 0.3$ mm s^{-1}) and a film coefficient $h = 30$ W m^{-2} K^{-1} corresponding

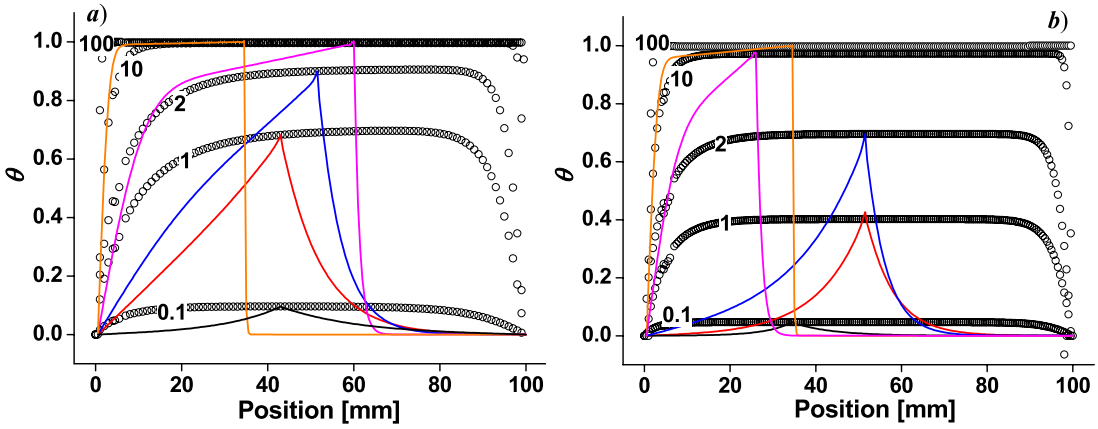

Figure 3. θ_{int} trends (black circles) and $\theta(x)$ profiles (color continuous lines) for several V_{ext} values ranging from 0.1 to 100 mm min^{-1} under different convection conditions: (a) $h = 30$ W m^{-2} K^{-1}; (b) $h = 130$ W m^{-2} K^{-1}. (Figures over the θ_{int} curves indicate V_{ext} values in mm min^{-1}.)

to natural convection conditions. Continuous lines represent temperature profiles $\theta(x)$ at different time instants. Three of these curves (A, B, C) have been emphasized using wider red lines. The open circles in figure 2 represent the development of the temperature θ_{int} at the interface position as it sweeps the specimen from left to right. A steady state characterized by a temperature $\theta_{std} \approx 0.7$ is reached after the interface displaced a length of approximately 40 mm. Similar conclusions have been found in the work of Messner *et al* [31], where the length necessary for reaching steady state was denoted as l_{crit}. It should be noted however that toward the right end position (figure 2) the temperature decreases abruptly due to the imposed boundary condition. Because of this, the temperature profile shows higher temperatures behind the interface position in this region (curve C).

In figure 3(a), several θ_{int} trends were included for V_{ext} values ranging from 0.1 to 100 mm min^{-1} and a film coefficient $h = 30$ W m^{-2} K^{-1}. It can be observed that, as V_{ext} increases, higher θ_{std} values are computed. It can be seen that for $V_{ext} = 10$ mm min^{-1} an adiabatic situation is already reached. In this case $\theta_{std} = 1$. Analysis of the figure also shows that the transient stage is more extended for intermediate values of V_{ext}, while for $V_{ext} = 100$ mm min^{-1} a $\theta_{std} = 1$ is reached almost instantaneously. In figure 3(b) the analysis performed in figure 3(a) is repeated, but now considering a film coefficient $h = 130$ W m^{-2} K^{-1}. For similar values of V_{ext}, lower values of θ_{std} and a shorter transient stage are now obtained.

Figures 3(a) and (b) also include representative temperature profiles $\theta(x)$ (colored continuous lines) for every value of V_{ext} once the corresponding θ_{std} has been reached. At low V_{ext} values, the $\theta(x)$ are quite symmetric with respect to the interface position. This situation evolves as V_{ext} increases. For $V_{ext} = 100$ mm min^{-1} the profiles can be approximated with a step function at the interface position. For this condition, there is not enough time for the heat released at the interface to be dissipated and local adiabatic conditions are therefore reached (i.e., latent heat is transformed completely into sensible heat at the interface).

Figure 4(a) shows a complete picture of the effect of both V_{ext} and h on the values of θ_{std}. Results were grouped according to the value of the film coefficient h considered. For each curve, the range of V_{ext} values for which the situation can be assumed as isothermal ($\theta_{std} \approx 0$) or adiabatic ($\theta_{std} \approx 1$) can be identified. They are separated by a transition range that covers approximately 1.5 decades in V_{ext}. It can be seen that increasing the h value shifts this transition toward higher V_{ext} values, as expected.

Similar behavior will be obtained for the magnitude of the temperature change in the case of the reverse transformation with the deviations being now negative due to the endothermic character of the reverse martensitic transformation. For an A–M interface which at a certain time will have an associated temperature θ_{int}, equation (9) indicates that the forward transformation will keep occurring at that interface whether the applied stress reaches a value $\sigma_{A-M} = \sigma_{A-Mref} + \beta(T_{int} - T_{ref})$ with T_{int} and θ_{int} related by equation (16). A similar conclusion can be reached for the reverse transformation where σ_{M-A} and T_{int} are now related by equation (10). Thus, it can be seen that the overloading (underloading) stress necessary for the forward (reverse) transformation is proportional to θ_{int}. The thermal effect contribution to the dissipated energy would be assessed as twice the area under the θ_{int} curve. It would be then expected that the dissipated energy exhibits the type of V_{ext} dependence shown in figure 4(a). This evaluation, though simple, is not correct, because in an actual complete cycle, the initial condition for the reverse transformation is not simply T_{amb}. Actually, the temperature level depends on the final temperature profile developed during the previous forward transformation and on the time elapsed during elastic unloading before reaching the corresponding critical stress for the reverse transformation. Therefore, an appropriate assessment of the thermal effect contribution has to be done in terms of the following integral evaluated over a complete cycle:

$$I = \oint \theta_{int} dZ. \tag{17}$$

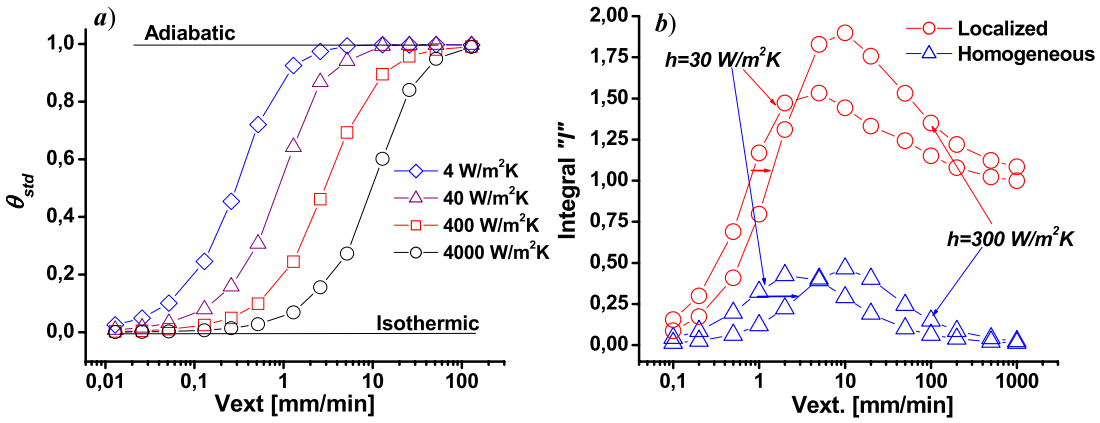

Figure 4. Thermal effects calculated as a function of V_{ext} and different values of film coefficient h. (a) Stationary interface adimensional temperature. (b) Total thermal contribution to the hysteresis energy given by the integral I.

This integral was evaluated numerically and it includes the forward transformation, a period of time (inversely proportional to V_{ext}) corresponding to the elastic unloading and the reverse transformation. Results are represented in figure 4(b). The curves with circles show that the integral I exhibits a maximum value for intermediate values of V_{ext} and that maximum location and its value depends on the convective conditions. The existence of this maximum is an experimental aspect correctly reproduced by the model so far developed.

The model predicts an asymmetric contribution to the hysteresis; i.e., on the adiabatic side (on the right of the maximum) the integral I reaches higher values than on the isothermal side of the maximum (on the left of the maximum). These last features however are contrary to the more symmetric bell shaped curves obtained from experiments reported in [19–22] where the dissipated energy on the adiabatic side drops to values as low as, or even lower than, on the isothermal side. The observed experimental dependence on V_{ext} can be understood if the transformation is assumed to proceed in a homogeneous rather than a localized way in the range of high V_{ext} values. This was shown by He *et al* [28] employing an analytical model. The numerical algorithm proposed in the present work can be easily adapted for the description of a homogeneous transformation, and by doing so the bell shaped curves could also be reproduced. This can be appreciated in figure 4(b), where curves with open triangle symbols were included to represent this condition. Therefore, the strain rate dependence of the hysteresis seems to be explained more satisfactory by a homogeneous transformation model in the high V_{ext} range. At first, this explanation for this behavior can be considered contrary to the experimental evidence, which clearly indicates that stress induced transformations in NiTi proceed in a localized manner. This discrepancy is however only apparent because there is still an important fact that has not yet been considered. This is related to the occurrence of nucleation events, which increases the number of active interfaces as V_{ext} increases. A high number of dispersed active interfaces would closely correspond to a situation of homogeneous transformation. In such situations, the individual interfaces would move more slowly for the same global transformation rate according to equation (13).

4. Criterion for the nucleation of a new phase domain

To this point, the proposed model could be implemented if the number and the initial position of interfaces are given. No mention has been made, so far, of where and when new transformations fronts appear. As stated in the introduction section, the localized character of the stress induced transformation has its origin in the particular stress state generated around an A–M interface. The consequence of this is that under uniaxial quasi-static conditions the applied stress required to nucleate an additional isolated martensite plate is higher than the stress needed to propagate a preexisting interface. The necessary overstress has a magnitude $\Delta\sigma_{nuc}$. For completeness, the criteria adopted in the present work for the assessment of $\Delta\sigma_{nuc}$ under isothermal conditions (quasi-static straining) will be explained in what follows. First, it is worthwhile to mention here that in the case of SMA superelastic wires the nucleation of martensite already occurs during the gripping procedure due to the associated stress concentration in the contact zone between specimen and grips. Therefore, once the critical stress σ_{A-M} is reached, the preexistent fronts propagate into the specimen. Because of this, no clear detection of nucleation is usually observed under direct gripping conditions. If, instead of using the plain wire, the specimen is thinned in the central part, favorable conditions for nucleation events taking place out of the grip zone could be obtained. In this way $\Delta\sigma_{nuc}$ can be evaluated. Figure 5 shows the results of such an experiment where a superelastic NiTi wire of diameter 2.5 mm and 70 mm in length (SAES Getters) was used. A central part thinned dog-bone specimen was obtained by spark eroding. The initial diameter was reduced to 1.75 mm in a 35 mm central part. An extensometer 25 mm in gage length was attached to the reduced section for strain measurement. In order to avoid the influence of thermal effects, the test was conducted at $V_{ext} = 0.1$ mm min^{-1}, which, according to previous experimental evidence, was shown to approach the isothermal

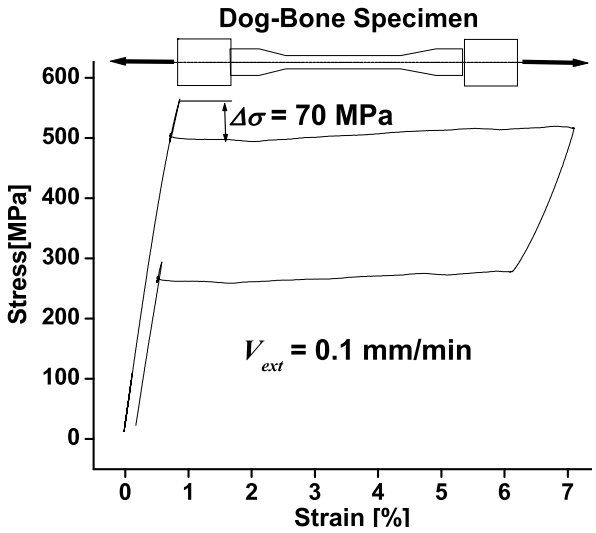

Figure 5. Superelastic cycle obtained from a NiTi dog-bone specimen. Martensite nucleates in the thinned zone, needing an overstress $\Delta\sigma_{\text{nuc}} = 70$ MPa.

regime for the present test conditions. A clear overstress $\Delta\sigma_{\text{nuc}}$ value of approximately 70 MPa was obtained from these experiments, as is illustrated in figure 5. In this case, the reverse transformation was induced before the forward transformation was completed, thus resulting in the absence of an austenite nucleation event in this case. Results of similar experiments performed in a fully transformed specimen indicate that a value of similar magnitude is obtained for the understress necessary for austenite nucleation. Considering a Clausius–Clapeyron coefficient $\beta = 7$ MPa K^{-1}, an equivalent temperature nucleation overheating (undercooling) of 10 K will be necessary for the nucleation of a new martensitic (austenitic) domain.

With the value of $\Delta\sigma_{\text{nuc}}$ determined for the isothermal conditions, the criterion for the nucleation of a new phase domain under dynamic conditions can be formulated: the nucleation condition will be reached when the difference between the temperature T_{int} at a propagating interface temperature and the minimum temperature T_{cool} in an austenite domain is equal to the equivalent temperature nucleation threshold of 10 K. Once the nucleation of a new domain occurs, two new active interfaces are added to those already existing. Analogously, during reverse transformation, the temperature will decrease around a propagating interface until an equivalent critical undercooling of 10 K is reached with respect to a hotter position in the martensitic phase. In this case, a new austenite domain will be nucleated.

5. Residual strain

The last aspect of the model to be explained has to do with the residual strain appearing at the end of the cycle in figure 5. Even though the origin and evolution of such strains are not among the main explored issues in this stage of the model, they were included for completeness with the aim of obtaining more realistic σ–ε curves. Residual strain ε_{r} is included as a new component of the total strain, by modifying equation (4) in the following way:

$$\varepsilon = \sigma/E_{\text{eff}} + Z\varepsilon_{\text{t}} + \varepsilon_{\text{r}}. \tag{18}$$

The introduction of ε_{r} makes it necessary also to modify equation (6) for the evaluation of phase portion Z. Thus

$$Z\,(\sigma, \varepsilon - \varepsilon_{\text{r}}) = \frac{(\varepsilon - \varepsilon_{\text{r}}) - (\sigma/E_{\text{A}})}{(\sigma/E_{\text{M}}) - (\sigma/E_{\text{M}}) + \varepsilon_{\text{t}}}. \tag{19}$$

The accumulation of this strain is related to the decrease in transformation stresses frequently observed during the first hundred cycles, referred to as the stabilization stage (see e.g. [22]). Both effects are known to evolve asymptotically with cycling. In the present work, attention will be focused only on the first complete cycle. In this case, ε_{r} can be calculated as

$$\varepsilon_{\text{r}} = \varepsilon_{\text{rmax}} Z_{\text{max}} \tag{20}$$

where e_{rmax} is the maximum residual strain corresponding to a fully transformed specimen and Z_{max} is the maximum reached phase portion. More detailed information can be found in [35].

6. Implementation of the thermomechanical model

With the basic mechanical model, the numerical scheme for the temperature field evaluation and the criterion for new phase domain nucleation as a background, it is possible to formulate an improved 1D superelasticity model able to deal with the thermomechanical coupled response. The calculus procedure for evaluation of the superelastic response can be summarized as follows.

(1) Evaluation of temperature field using equation (14).
(2) Updating of critical stresses $\sigma_{\text{A–M}}$ and $\sigma_{\text{M–A}}$ using equations (9) and (10). The value of T is assumed to correspond to the temperature of the interface which has the lowest (highest) temperature for the computation of $\sigma_{\text{A–M}}$ ($\sigma_{\text{M–A}}$).
(3) Seeking for nucleation events. It is evaluated whether a temperature difference -10 K ($+10$ K), equivalent to $\Delta\sigma_{\text{nuc}} = 70$ MPa (-70 MPa), exists between the temperature of the hottest (coolest) interface evaluated in step 2 and the temperature of any austenite (martensite) node. If this condition is fulfilled, the nucleation of a new domain will take place (instead of the propagation of one of the existing interfaces). If a nucleation event is determined to occur, $\sigma_{\text{A–M}}$ and $\sigma_{\text{M–A}}$ have to be re-defined according to the temperature at the position where the new interfaces appear.
(4) Computation of a new σ–ε state. It is evaluated whether a new strain increment $\Delta\varepsilon$ can be accommodated either elastically or through a variation of the phase portion Z. These will be achieved by the propagation of one of the interfaces selected in step 2 or the nucleation of a new domain determined in step 3. Eventually, the computed phase changes will be the input for the temperature evaluation of the next calculus cycle.

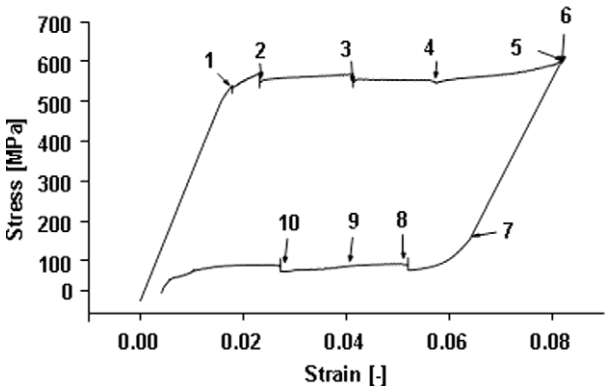

Figure 6. Simulated σ–ε curve. Arrows denote successive nucleation and collapse events. $V_{ext} = 1.5$ mm min^{-1}, $h =$ 15 W m^{-2} K^{-1}, $L = 500$ mm, $d = 2.5$ mm, $T_{amb} = 25\,^{\circ}$C.

7. Results

In first place, the model was implemented to study nucleation events for different values of V_{ext} and environment conditions. By adopting a discretization of $N = 400$ nodes for a wire of length $L = 500$ mm and diameter $d = 2.46$ mm, for a maximum strain of 0.08, several superelastic cycles were simulated. The following materials properties were assumed: $E_A = 32$ MPa, $E_M = 25$ GPa, $\varepsilon_t = 0.05$; transformation stresses for reference temperature $T_{ref} = 25\,^{\circ}$C, $\sigma_{A–Mref} =$ 500 MPa and $\sigma_{M–Aref} = 100$ MPa; $T_{amb} = 25\,^{\circ}$C. The maximum residual strain value ε_{rmax} was set at 0.0015. For these simulations a film coefficient $h = 15$ W m^{-2} K^{-1}, corresponding to stagnant air, is assumed. Figure 6 shows the σ–ε curve obtained for a cycle performed with an imposed $V_{ext} = 1.5$ mm min^{-1}, while in figure 7 the temperature profile $T(x)$ and the local phase fields $Z(x)$ during the complete cycle are included as colored contours (figures 7(a) and (b), respectively). Corresponding state points in figures 6 and 7(a) and (b) were identified (points 1 to 10) to facilitate the analysis. Initially, an interface is introduced at the lower end of the specimen. Its preexistence is assumed due to the stress state caused by the clamps. This interface starts moving upwards into the specimen length as soon as the stress resulting from the imposed displacement reaches the critical stress $\sigma_{A–M} = \sigma_{A–Mref} = 500$ MPa given by equation (9) (initially, $T = T_{amb} = 25\,^{\circ}$C $= T_{ref}$). At point 1 (357 s), immediately after the transformation onset, a second interface nucleates at the upper end of the specimen. At point 2 (530 s), the nucleation of two new interfaces take place. Thus, four interfaces move now until point 3 (840 s), where two additional interfaces nucleate. It can be appreciated from the slope of the limiting lines of the phase fields in figure 7(b) that each time a new interface appears the mean interface velocity decreases. At point 4 (1134 s) the collapse of two fronts occurs, while at point 5, close to the end of the forward transformation, another two fronts collapse. The occurrence of all the mentioned nucleation/collapse events is associated with a corresponding stress step in the σ–ε curve shown in figure 6. From point 4 on, the temperature profiles of the different fronts begin to overlap and temperatures as high as 48 °C are

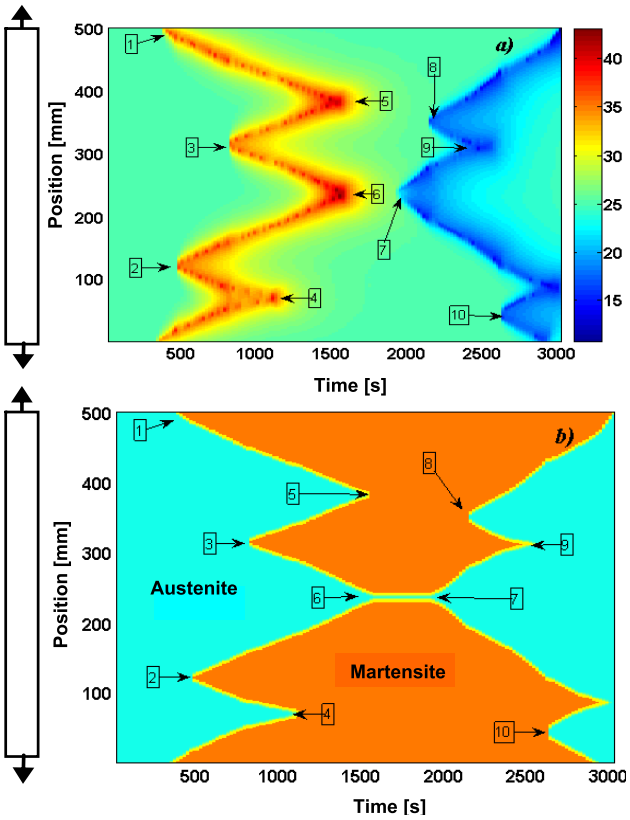

Figure 7. (a) Temperature and (b) phase portion Z fields corresponding to the simulation of the cycle of figure 6: $V_{ext} = 1.5$ mm min^{-1}, $h = 15$ W m^{-2} K^{-1}. $L = 500$ mm, $d = 2.5$ mm, $T_{amb} = 25\,^{\circ}$C (the right inset in (a) corresponds to the temperature scale in °C).

reached. During unloading, the reverse transformation starts at point 7 (2000 s). The fronts which did not collapse at the end of the straining stage now reverse their movement. At point 8 (2230 s), the nucleation of an austenite domain occurs. Two new fronts are then active. At point 9 (2400 s), the collapse of two interfaces occurs. The reduction in the number of active interfaces produces an increase in the velocity of the remaining interfaces. A corresponding decrease in stress is observed (figure 6). At point 10 (2720 s), a new austenite nucleation event occurs. Two new additional interfaces now participate in the reverse transformation process. It can be seen that toward the end of the unloading stage the collapse of two of the interfaces results in a temperature decrease of 11 °C with respect to T_{amb}.

The effect of increasing the velocity V_{ext} from 1.5 to 100 mm min^{-1} is now considered. Figure 8(a) shows the simulated mechanical response while figure 8(b) illustrates the corresponding temperature field evolution. As in the previous case, a clear correspondence between the features associated with the nucleation events in both figures can be appreciated. It can be seen that initially, until approximately 13.5 s, the nucleation events are regularly distributed along the length of the specimen. After this, the thermal interaction between the individual fronts results in a rather homogeneous temperature profile which inhibits further nucleation events. This corresponds to the monotonic increase in stress observed

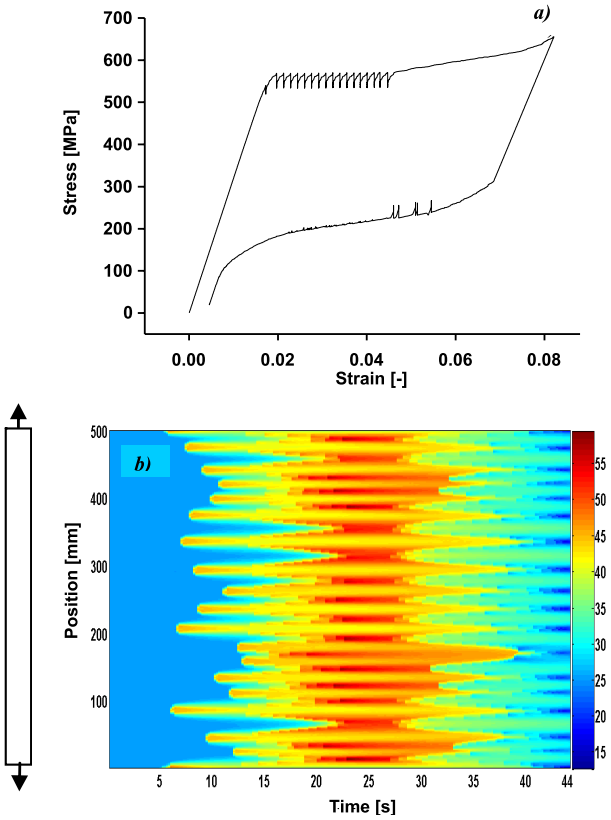

Figure 8. Simulated superelastic cycle at $V_{ext} = 100$ mm min^{-1}, $h = 15$ W m^{-2} K^{-1}, $L = 500$ mm, $d = 2.5$ mm, $T_{amb} = 25\,^{\circ}$C. (a) σ–ε curve. (b) Temperature field evolution during the cycle. (The right inset in (a) corresponds to the temperature scale in °C.)

in the second half of the forward transformation branch in figure 8(a). The maximum temperature reached at specific positions during forward transformation is now close to 60 °C. It is important to note here that this 35 °C deviation from T_{amb} is higher than the maximum deviation of 18 °C obtained in the case of the single interface propagating under adiabatic conditions described in section 3. During the reverse transformation, the temperature decreases to 12 °C at the points where interfaces collapse.

In figure 9, experimental and numerical results corresponding to σ–ε curves for three different values of V_{ext} are compared. Commercial superelastic NiTi wires (SAES Getters) with a diameter $d = 2.46$ mm were used in the experiments. For the numerical simulations a mesh with $N = 200$ nodes was employed. A value of $h = 15$ W m^{-2} K^{-1} (still air) was considered appropriate in this case. It can be seen that there is a reasonable agreement between the experimental and the simulated σ–ε behavior. The implemented model is able to reproduce the main qualitative aspects of real cycles, including the presence of stress drops associated with the appearance of new fronts and the inclination of the plateau, which is related to the temperature variation due to self-heating during forward transformation or self-cooling during reverse transformation effects.

Finally, the model was applied to the study of the relationship between the strain rate and the number of transformation domains. Results from previous work performed by Zhang *et al* [17] and He *et al* [28] were used here as benchmark cases. These authors studied both experimentally and analytically the strain rate dependence of the hysteresis. To facilitate the comparisons, the same specimen geometry and parameters were considered, i.e., a NiTi strip 30 mm in length, 2.6 × 0.5 mm in cross section, $\Delta\sigma_{nuc} = 18$ MPa, $\varepsilon_t = 0.047$ and $h = 10$ W m^{-2} K^{-1}. Values for $\sigma_{A–Mref} = 400$ MPa and $\sigma_{M–Aref} = 140$ MPa were taken from results corresponding to the isothermal experiments reported in figure 9.1 from [17]. For the simulations performed in the present work, V_{ext} values in the range from 0.05 to 600 mm min^{-1} were employed. The calculated σ–ε curves are shown in figure 10(a). Strain rate values were also included in the figure; they were calculated from V_{ext} and the length of the specimen to allow a direct comparison with results shown in figure 9(a) from [17]. The shape of the calculated σ–ε curves reproduces the trends observed experimentally. Figure 10(b) shows the mean value of the mean stress hysteresis plotted as a function of the velocity V_{ext} (alternatively, strain rate) for h values of 10 and 100 W m^{-2} K^{-1}. Following the procedure described in [17], the mean stress hysteresis was computed by dividing the whole area enclosed in the superelastic loop by the transformation strain. The calculated values exhibit reasonable agreement with those obtained experimentally.

It is worthwhile noticing here that the bell shape curve associated with the thermal contribution dependence on V_{ext} and the homogeneous transformation analysis of section 3 is now obtained under the assumption of localized transformation and a varying number of interfaces.

The model implemented in the present work allows calculation of different parameters associated with the pseudoelastic behavior under dynamic conditions. Figure 11 shows the maximum number of active interfaces as a function of V_{ext} for the case just described. It can be seen that, in the intermediate range, the calculated results are in line with the 0.5 potential dependence obtained from the experiments reported in [17]. They are also in line with the results corresponding to the analytical solutions presented in [36]. As can be expected, the 0.5 potential dependence breaks down as V_{ext} gets higher due to the exhaustion of the space available for further nucleation events. This is related to the finite spatial width associated with an interface, a feature which is adequately captured by the model proposed in the present work.

8. Summary and conclusions

A thermomechanical model intended to be used as a design tool for applications of the superelastic effect exhibited by 1D NiTi shape memory elements (wires and ribbons) was developed. The basic mechanical model assumes the global response of a specimen results from the serial connection of austenite and martensite elemental volumes and includes the temperature dependence of the

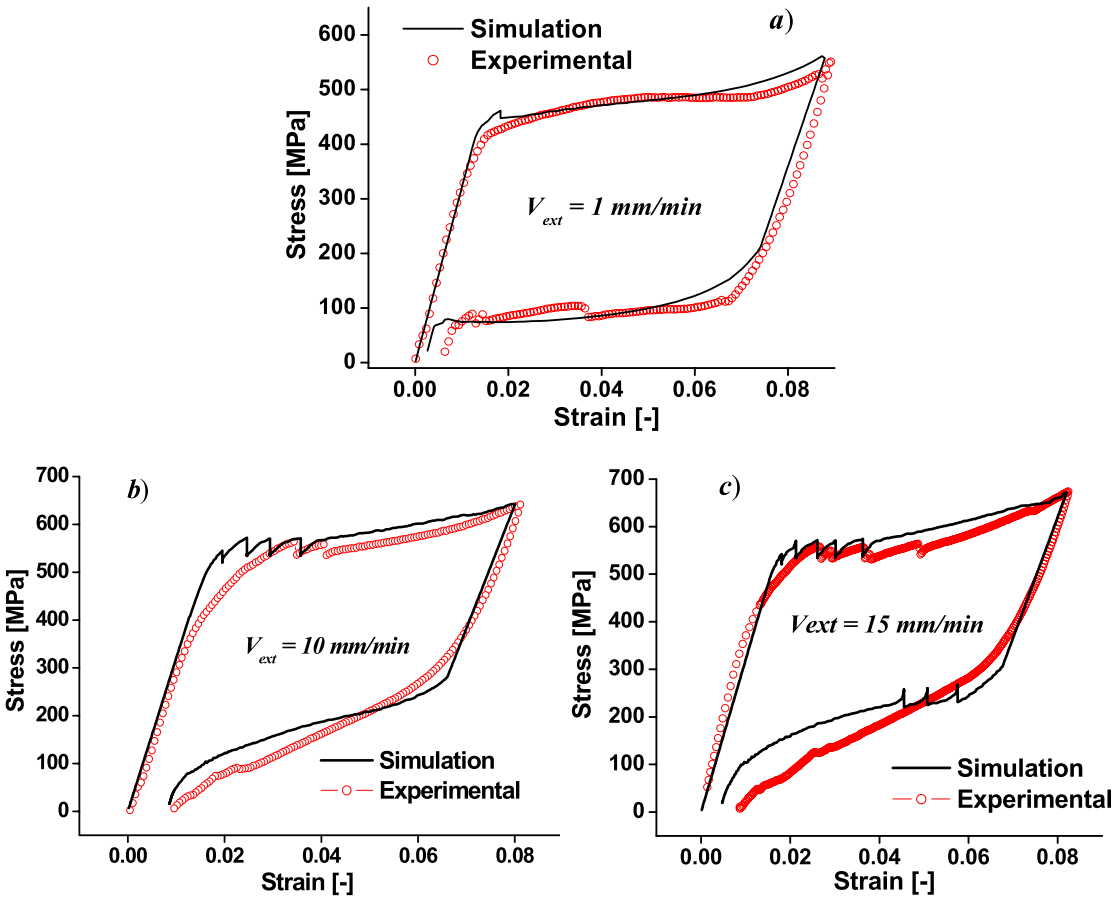

Figure 9. Comparison between experimental and simulated σ–ε curves for NiTi wires of $d = 2.46$ mm. (a) $V_{\text{ext}} = 1$ mm min^{-1}, $L = 91$ mm. (b) $V_{\text{ext}}t = 10$ mm min^{-1}, $L = 75$ mm. (c) $V_{\text{ext}} = 15$ mm min^{-1}, $L = 94$ mm. Simulations were made with a coefficient $h = 15$ W m^{-2} K^{-1} and $T_{\text{amb}} = 25\,^{\circ}$C.

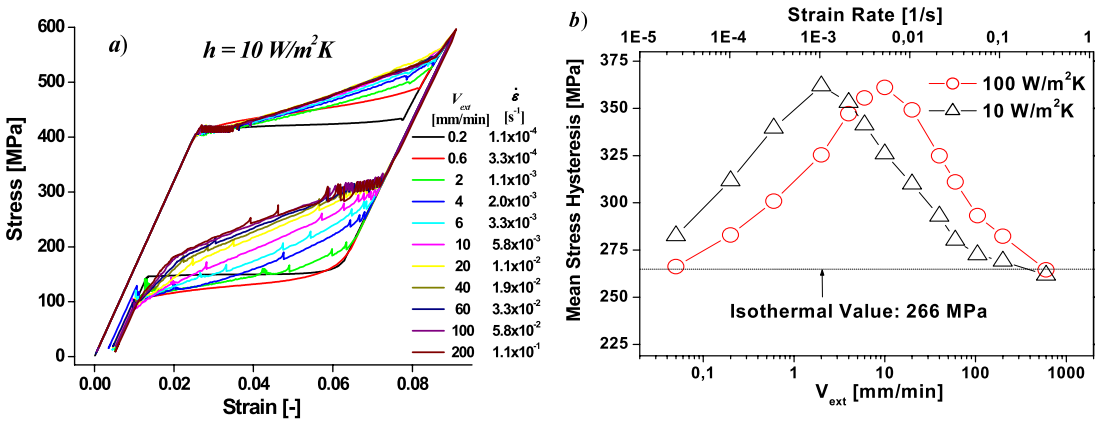

Figure 10. Simulated superelastic cycles with V_{ext} values ranging from 0.05 to 600 mm min^{-1}. Specimen geometry and parameters were taken from the experimental work reported in [17]. (a) σ–ε curves obtained with a film coefficient $h = 10$ W m^{-2} K^{-1}. (b) Mean stress hysteresis of the cycles as a function of V_{ext} or the corresponding strain rate for two ambient conditions: $h = 10$ W m^{-2} K^{-1} (still air) and $h = 100$ W m^{-2} K^{-1} (5 m s^{-1} air flow velocity).

critical transformation stresses. This basic mechanical model, together with a scheme for calculating the temperature along the specimen, a criterion for the nucleation of new transforming/retransforming domains and a simplified algorithm to compute residual strains, were assembled to constitute a coupled 1D thermomechanical model of the superelastic behavior.

Numerical predictions obtained with the model were contrasted with experimental results from different sources. The simulations performed allowed rationalization of different

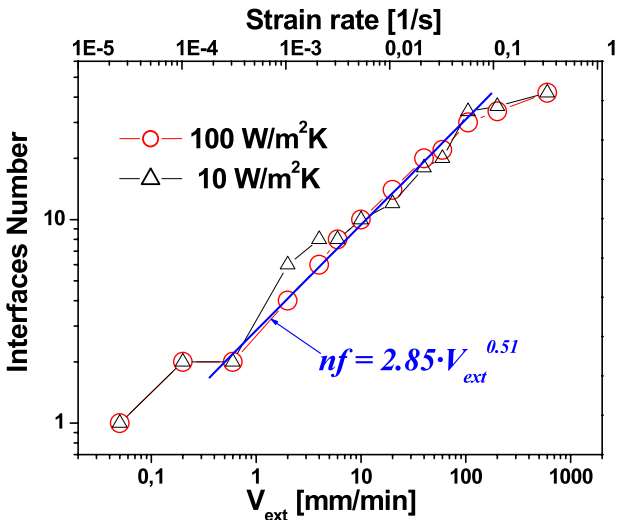

Figure 11. Maximum number of active interfaces as a function of V_{ext} obtained from simulations.

features observed in experiments and their dependence on strain rate and environment conditions.

Considering its simplicity and the wide range of conditions of applicability, the model introduced in the present work constitutes an interesting tool to be used in a design stage for the evaluation of different properties associated with the superelastic effect exhibited by NiTi shape memory alloys.

Acknowledgments

Funding from project PICT 2284-07 (ANPCyT) and program SECTyP 2010–2014 (UNCuyo) is acknowledged. HS also acknowledges CONICET for financial support.

References

[1] Otsuka K and Wayman C 1998 *Shape Memory Materials* (Cambridge: Cambridge University Press)
[2] Wollants P, Roos J R and Delaey L 1993 Thermally and stress induced thermoelastic martensitic transformations in the reference frame of equilibrium thermodynamics *Prog. Mater. Sci.* **37** 227–88
[3] Wilson J C, Eeri M and Wesolowskya M J 2005 Shape memory alloys for seismic response modification: a state-of-the-art review *Earthq. Spectra* **21** 569–601
[4] Masuda A and Noori N 2002 Optimization of hysteretic characteristics of damping devices based on pseudoelastic shape memory alloys *Int. J. Non-Linear Mech.* **37** 1375–86
[5] Dolce M, Cardone D and Marnetto R 2000 Implementation and testing of passive control devices based on shape memory alloys *Earthq. Eng. Struct. Dyn.* **29** 945–68
[6] Des Roches R and Delemont M 2002 Seismic retrofit of simply supported bridges using shape memory alloys *Eng. Struct.* **24** 325–32
[7] Duerig T W, Melton K N, Stöckel D and Wayman C M 1990 *Engineerig Aspects of Shape Memory Alloys* 1st edn (London: Butterworth-Hinemann)
[8] Otsuka K and Ren X 2005 Physical metallurgy of Ti–Ni-based shape memory alloys *Prog. Mater. Sci.* **50** 511–678
[9] Patoor E, Lagoudas D C, Entchev P B, Brinson L C and Gao X 2006 Shape memory alloys, part I: general properties and modeling of single crystals *Mech. Mater.* **38** 391–429
[10] Shaw J and Kyriakides S 1997 On the nucleation and propagation of phase transformation fronts in a NiTi alloy *Acta Mater.* **45** 673–700
[11] Churchill C, Shaw J and Iadicola M 2009 Tips and tricks for characterizing shape memory alloy wire: part 2, fundamental isothermal responses *Exp. Tech.* **2** 51–62
[12] Sittner P, Liu Y and Novak V 2005 On the origin of Lüders-like deformation of NiTi shape memory alloys *J. Mech. Phys. Solids* **53** 1719–46
[13] Tan G, Liu Y, Sittner P and Saunders M 2004 Lüders-like deformation associated with stress-induced martensitic transformation in NiTi *Scr. Mater.* **50** 193–8
[14] Sun Q and Zhong Z 2008 An inclusion theory for the propagation of martensite band in NiTi shape memory alloy wires under tension *Int. J. Plast.* **16** 1169–87
[15] Zhong Z, Sun Q and Tong P 1999 On the elastic axisymmetric deformation of a rod containing a single cylindrical inclusion *Int. J. Solids Struct.* **37** 5943–55
[16] Iadicola M and Shaw S 2008 The effect of uniaxial cyclic deformation on the evolution of phase transformation fronts in pseudoelastic NiTi wire *J. Intell. Mater. Syst. Struct.* **13** 143–55
[17] Zhang X, Feng P, He Y, Yu T and Sun Q 2010 Experimental study on rate dependence of macroscopic domain and stress hysteresis in NiTi shape memory alloy strips *Int. J. Mech. Sci.* **52** 1660–70
[18] Isalgue A, Torra V, Yawny A and Lovey F C 2008 Metastable effects on martensitic transformation In SMa, Part VI, The Clausius–Clapeyron relationship *J. Therm. Anal. Calorimetry* **91** 991–8
[19] Piedboeuf M C and Gauvin R 1998 Damping behaviour of shape memory alloys, strain amplitude, frequency and temperature dependence effects *J. Sound Vib.* **214** 885–901
[20] Heller L, Sittner P, Pilch P and Landa M 2009 Factors controlling superelastic damping capacity of SMAs *J. Mater. Eng. Perform.* **18** 603–11
[21] He Y, Yin Y, Zhou R and Sun Q 2010 Ambient effect on damping peak of NiTi shape memory alloy *Mater. Lett.* **64** 1483–6
[22] Soul H, Isalgue A, Yawny A, Torra V and Lovey F C 2010 Pseudoelastic fatigue of niti wires: frequency and size effects on damping capacity *Smart Mater. Struct.* **19** 085006
[23] Cormick Mc, DesRosches R, Fugazza D and Auricchio F 2006 Seismic vibration control using superelastic shape memory alloys *J. Eng. Mater. Technol.* **128** 294–301
[24] Trochu F and Terriault P 1998 Nonlinear modelling of hysteretic material laws by dual kriging and application *Comput. Methods Appl. Mech. Eng.* **151** 545–58
[25] Saadat S, Noori M, Davoodi H, Hou Z, Suzuki Y and Masuda A 2001 Using NiTi SMA tendons for vibration control of coastal structures *Smart Mater. Struct.* **10** 695–704
[26] Gall K, Lim T, McDowell D, Sehitoglu H and Chumlyakov Y 2000 The role of intergranular constraint on the stress-induced martensitic transformation in textured polycrystalline NiTi *Int. J. Plast.* **16** 1189–214
[27] Manchiraju S and Anderson P 2010 Coupling between martensitic phase transformations and plasticity: a microstructure-based finite element model *Int. J. Plast.* **26** 1508–27
[28] He Y J and Sun Q P 2011 On non-monotonic rate dependence of stress hysteresis of superelastic shape memory alloy bars *Int. J. Solids Struct.* **48** 1688–95
[29] Maletta C, Falvo A, Furgiuele F and Reddy J 2009 A phenomenological model for superelasticity in NiTi alloys *Smart Mater. Struct.* **18** 025005
[30] Morin C, Moumni Z and Zaki W 2011 A constitutive model for shape memory alloys accounting for thermomechanical coupling *Int. J. Plast.* **27** 748–67

[31] Messner C and Werner E 2003 Temperature distribution due to localised martensitic transformation in SMA tensile test specimens *Comput. Mater. Sci.* **26** 95–101
[32] Iadicola M and Shaw J 2004 Rate and thermal sensitivities of unstable transformation behavior in a shape memory alloy *Int. J. Plast.* **20** 577–605
[33] Incropera F and DeWitt D 1996 *Fundamentals of Heat and Mass Transfer* 4th edn (Toronto: Wiley)
[34] Richard L, Burden J and Faires D 1998 *Análisis Numérico* (Mexico: International Thomson Editors)
[35] Soul H and Yawny A 2012 Superelastic behaviour of NiTi wires under general cycling conditions: thermomechanic 1-D modeling *Procedia Mater. Sci.* **1** 141–8
[36] He Y and Sun Q 2010 Rate-dependent domain spacing in a stretched NiTi strip *Int. J. Solids Struct.* **47** 2775–83